Journal of Marine Research, 73, 33–48, 2015

A composite vertical current spectrum for strongly and weakly stratified seas and oceans

by Hans van Haren[1]

ABSTRACT

An overall frequency (σ) spectrum $\Phi_w(\sigma, N, f_h)$ is composed for vertical current (w) observations from ocean areas with different stratifications represented by large, 100 m scale buoyancy frequency N. The horizontal Coriolis parameter is denoted by f_h. In the open Atlantic Ocean, the relatively strong horizontal layering in density supports the Φ_w that is found in semiequilibrium under the degradation of the lowest internal wave mode. This Φ_w is not constant with frequency; however, its variance increases between $\sigma = f$ and its peak near $\sigma = (0.5{-}0.7)N >> f$, where f denotes the local inertial frequency. In contrast, the Φ_w spectra from the weakly stratified deep Mediterranean and from the shallow North Sea peak at $\sim 1.1f$, except for a tidal peak in North Sea data, and fall off at a rate of σ^{-1} for $1.1f < \sigma < N_m = 4f_h$, where N_m denotes maximum small-scale N. Background conditions are characterized by vertical instead of horizontal layering in density. Such spectra are best described by a nonequilibrium evolution of small-scale internal waves under a weak mean shear, which transfers variance to $\sigma \approx f$. This $\Phi_w \sim N^p$, $p > 0$, is contrary to the existing model of open-ocean equilibrium spectra that decrease with N ($p < 0$). A smooth transition between the two regimes is found to coincide with top-peak Φ_w for $N/f_h = 4$.

Keywords. composite ocean spectrum, vertical motions, internal waves, weak and strong stratification, mixing effects

1. Introduction

The ocean is stably stratified in the vertical, yet in constant motion by internal waves supported by these density variations. Several sources of internal waves have been identified, varying from geostrophic adjustment following sudden disturbances to tide-topography interaction (e.g., LeBlond and Mysak 1978). Far from sources, perhaps after multiple interactions within the wave field, one might expect to find an equilibrium spectrum of multimode isotropic internal waves (Garrett and Munk 1972, 1979; Munk 1981). Such an equilibrium spectrum describes a balance between large-scale forcing and small-scale dissipation. The dissipation is governed by a balance between the stabilizing stratification and the destabilizing shear. However, both near boundaries and in the open ocean, large variations in

1. Royal Netherlands Institute for Sea Research (NIOZ), P.O. Box 59, 1790 AB Den Burg, The Netherlands. ***e-mail: hans.van.haren@nioz.nl***

© 2015 Hans van Haren.

stratification and other environmental conditions may occur, thus challenging the balance. For example, stratification and shear are in general large across thin interfaces that may result from internal wave straining or breaking (e.g., Linden 1979). (Thin interfaces reflect a relatively large change in density across a small vertical distance. Together with thicker weakly stratified layers above and below, they create a "steppy" layering of density, which contrasts with a smoothly varying ocean density profile generally adopted in models.) As suggested by Wunsch (1975), a nonequilibrium internal wave field may exist close to sources such as near-bottom topography. In the ocean interior, thin interfaces and weakly stratified layers may be amongst these areas or indicative of such wave fields.

Here, different internal wave regimes are investigated varying from very weak to strong stratification. It may be shown that only waves at the inertial frequency f can freely propagate between strongly stratified and completely homogeneous layers (LeBlond and Mysak 1978). During such propagation, the governing inertia-gravity wave dynamics change from mainly gravity driven to mainly momentum driven as a result of Earth's rotation. In the weakly stratified layers, the Coriolis parameter f_h can no longer be neglected. It results in relatively large convective motions in the direction of Earth's rotational vector (van Haren and Gostiaux 2011).

Instead of a smooth transition between zero and nonzero stratification, convection away from gravity in the direction of Earth's rotational vector leads to three abrupt transitions from zero to minimum stable stratification, $N_{\min} = f_h, 2f_h$, and $4f_h$ under nonlinear, linear, and nonlinear stability conditions, respectively (van Haren 2008a). This extends the motions and shear to subinertial frequencies, thereby affecting internal wave–induced mixing. It is also expected that minimum stratification limits the internal wave frequencies.

To distinguish internal wave motions from others like barotropic tidal, it is best to observe the vertical current component representing interfacial displacements. Horizontal current components are less suitable because of a combination of factors: (1) the aspect ratio, although generally being 0.01–0.001 for large ocean motions, becomes $O(1)$ for internal waves near the buoyancy frequency in strong- and weakly stratified waters (Munk 1980; van Haren and Millot 2005); and (2) horizontal motions are dominated by large-scale barotropic currents, which are found in the internal wave band also in weakly stratified waters.

In this article, first some theoretical models are revisited on internal wave vertical current spectra. Subsequently, some examples of equilibrium and nonequilibrium internal wave fields are used to compose a general ocean spectrum from Eulerian moored observations that describe interface displacements under near-homogeneous and well-stratified conditions. This composite spectrum is inferred from directly observed vertical currents using the 75 kHz Long Ranger acoustic Doppler current profiler (ADCP). Such current observations are an adequate means to quantify internal waves' displacements, remotely sensed over a considerable vertical range of several hundreds of meters. The possible connection between the internal wave field's level of nonequilibrium and ocean mixing is discussed.

2. Theoretical vertical current spectra

Here, we review three model spectra that we take to represent equilibrium, semiequilibrium, and nonequilibrium wave regimes. Perhaps because of the difficulty of measuring vertical currents (w) in the ocean, few theoretical descriptions of internal wave w spectra exist. However, such spectra can be inferred from more common vertical displacement (η) spectra Φ_η, using the correspondence (e.g., Fofonoff 1969),

$$w = d\eta/dt \propto i\sigma\eta, \tag{1}$$

where w and η are complex amplitudes, σ denotes the wave frequency, and $i^2 = -1$.

The classic equilibrium displacement variance spectrum for freely propagating internal waves having frequencies $f << \sigma << N$ is (Munk 1981)

$$\Phi_\eta(\sigma, N) \propto fN^{-1}(\sigma^2 - f^2)^{1/2}\sigma^{-3}, \tag{2a}$$

which is approximated as

$$\Phi_\eta(\sigma, N) \propto N^{-1}\sigma^{-2}, \tag{2b}$$

where N denotes the large vertical-scale buoyancy frequency. An e-folding scale of 1,300 m defines the large-scale N; here, we use $\Delta z = 100$ m for such scales. The debatable f dependence in equation (2a) is removed in the approximation (2b) as, according to Munk (1980), potential energy (PE) density is generally found to be independent of latitude. The PE spectrum thus reads

$$\Phi_{\rm PE}(\sigma, N) = N^2\Phi_\eta \propto N\sigma^{-2}. \tag{3}$$

Combining equations (1) and (2b) gives a wave-frequency independent spectrum,

$$\Phi_w(\sigma, N) \propto N^{-1}\sigma^0 = N^{-1}, \tag{4}$$

in which variance decreases with increasing stratification.

Phillips (1966) suggested another internal wave spectrum model by using the condition of hydrodynamic instability for the degradation of the lowest internal wave mode across a sharp density interface (pycnocline). This condition reads in terms of gradient Richardson number, $Ri = N^2/|\mathbf{S}|^2 < Ri_{cr}$, where $\mathbf{S}$ denotes the shear vector and $Ri_{cr} = 0.25$ the necessary criterion for linear stability (Howard 1961; Miles 1961). Phillips's result distinguishes high-frequency "short" waves in the interfacial pycnocline and low-frequency "long" waves in the weaker-stratified layers outside the pycnocline, so that

$$\Phi_\eta(\sigma, N) \propto N^4 N_m^{-2}\sigma^{-3}, \qquad N << \sigma << N_m \tag{5a}$$

$$\Phi_\eta(\sigma, N) \propto N^2 N_m^{-2}\sigma^{-1}, \qquad [f <]\sigma << N \tag{5b}$$

where N_m denotes the maximum interfacial "small-scale" buoyancy frequency (Miropol'sky 2001). The inertial frequency is added here between square brackets; Phillips did not consider it. This condition reminds us that freely propagating internal waves do not exist for $\sigma < f$ on a rotating sphere under stratified conditions.

Using equation (1), equations (5a) and (5b) result in a wave-frequency dependent spectrum,

$$\Phi_w(\sigma, N) \propto N^4 N_m^{-2} \sigma^{-1}, \qquad N << \sigma << N_m \tag{6a}$$

$$\Phi_w(\sigma, N) \propto N^2 N_m^{-2} \sigma^{+1}. \qquad [f <] \sigma << N \tag{6b}$$

As equations (6a) and (6b) describe an internal wave field of which the lowest modes are degraded, we adopt them as a "semiequilibrium" spectrum.

A result for a nonequilibrium internal wave spectrum was obtained by Phillips (1966; not in later editions) considering the influence of relatively weak mean shear ($Ri > 0.25$ everywhere) on the evolution of internal waves with vertical scales that are small compared with the scales of mean shear and stratification. Such a shear reduces the frequency and vertical scale of small-scale internal waves. Without dissipation, energy is transferred to the "mean" low-frequency flow. This results in a time-dependent evolution of the internal wave field. In the case of an internal wave source like a region of turbulence with constant production of high-mode internal waves, this gives

$$\Phi_\eta(\sigma, N) \propto |\mathbf{S}|(N^2 - \sigma^2)^{1/2} \sigma^{-3}, \tag{7a}$$

$$\Phi_w(\sigma, N) \propto |\mathbf{S}|(N^2 - \sigma^2)^{1/2} \sigma^{-1}, \tag{7b}$$

in which the shear magnitude is retained here in purpose. Phillips (1966) added the condition $f << \sigma < N$ to equations (7a) and (7b), but this can be questioned given the previous transfer of energy from high to low internal wave frequencies and the small vertical scale of nearly horizontally propagating near-inertial motions (e.g., LeBlond and Mysak 1978) to which the initially high-frequency waves are refracted. It seems more appropriate to include near f in the frequency range. I therefore propose the alternative form of equation (7b) of a different wave-frequency dependence,

$$\Phi_w(\sigma, N) \propto N^2 \sigma^{-1}, \qquad f < \sigma << N \tag{8}$$

where a constant Ri is assumed so that $|\mathbf{S}| \propto N$.

With equations (4), (6a), (6b), and (8), we have three different theoretical wave-frequency slopes and N scalings for the internal wave spectrum Φ_w. These will be compared with observed spectra subsequently.

3. ADCP data and spectral processing

Although several single-point current meters exist that measure all three components of current (u, v, w), most direct vertical current measurements are made using acoustic current

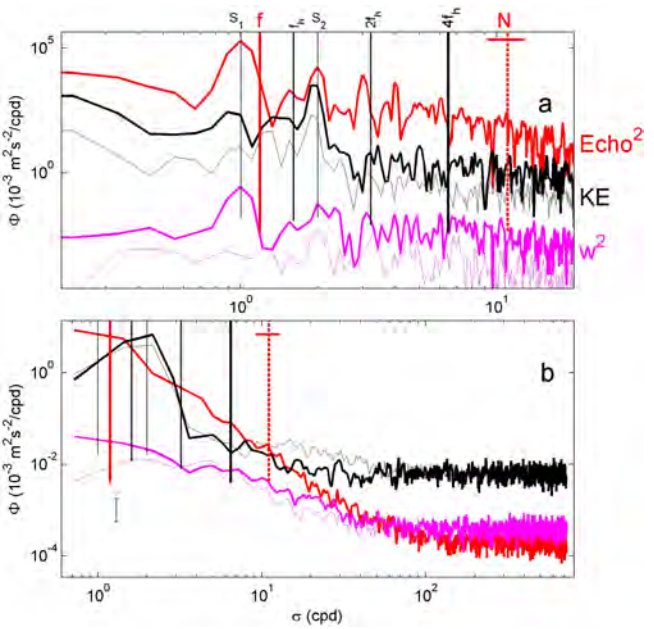

Figure 1. Spectral comparison of vertical currents (purple) with horizontal currents (black) and echo amplitude (red, arbitrary units) for a 9-day acoustic Doppler current profiler record from the central-north Alboran Sea. Thick-line spectra are from 285 m, and thin-line spectra from 540 m. (a) Nearly raw spectra with ∼3 degrees of freedom (dof) resolving dominant tidal, inertial, and other internal wave frequencies. Spectra are arbitrarily offset vertically, for clarity. (b) Moderately smoothed (∼15 dof) spectra focusing on the high-frequency tail. Spectra are not offset vertically. The vertical lines are at the same frequencies as in panel (a) and can be used for reference. The black vertical bar indicates the 95% confidence levels of random statistical significance. cpd, cycles per day; KE, kinetic energy.

profilers. ADCPs have the advantage that their beams are oriented at an angle of typically 20° from the vertical, so that the standard error in w is a factor of ∼3.5 smaller than the error in horizontal current components (u, v). A 75 kHz system ranges over 600 m vertically, over which background conditions like stratification may vary considerably. A disadvantage of ADCPs is that (u, v, w) are averaged over the beam spread, which can amount to several hundreds of meters horizontally over 600 m.

For the present analyses, ADCP time-series observations are used to compute power spectra. Prior to Fourier transform, a Kaiser taper window (Parks and Burrus 1987) is applied to the data. For smoothing, spectra are computed for half-overlapping segments and averaged. Examples of nearly raw (full-record-length segment) and moderately smoothed (1.5-day segments) spectra are given in Figure 1(a) and (b), respectively. These data of a 9-day time series from the weakly stratified Alboran Sea between Spain and Morocco (henceforth AS) are discussed in detail in Section 5.

During 9 days in April 2013, an upward-looking 75 kHz ADCP was moored ∼100 m above the bottom in 912 m water depth at 36°24′ N, 3°30′ W in the central-north AS. At this latitude, $f_h \approx 1.45$ cpd. The ADCP sampled currents and echo amplitudes at a rate of once per minute over a range of 600 m. For the raw 60 s sampled data, the noise level was ∼0.019 and 0.005 m s^{-1} for (u, v) and w, respectively. Using random statistics, these values are reduced by a factor of 7.5 for motions with 1 h periodicity. Every other day, a single Sea-Bird 911 conductivity-temperature-depth (CTD) profile was made within 1 km of the mooring.

In Figure 1(a), it is seen that the horizontal currents, dominating the kinetic energy (KE; black), peak at the semidiurnal lunar frequency because of deterministic barotropic tides. In contrast, the vertical currents (purple) at 285 m (thick line) peak at the diurnal frequency. This peak is due to solar diurnal vertical migrations by zooplankton, which are found above 400 m in this area and which are most visible in the acoustic echo amplitude (red). The square instead of sinusoidal form of these migratory motions is represented spectrally by a sequence of higher harmonics, visible in the echo and, to a lesser extent, w spectrum at 285 m.

In the same frequency range of a few cycles per day (hereafter cpd), w is found to extend above the flat white-noise level of zero slope, visible for $\sigma > 100$ cpd in Figure 1(b). There, the w variance is approximately a factor of $10 \approx 3.5^2$ smaller than that of KE, commensurate with the difference in standard error as provided by the manufacturer. At ∼6 cpd, the w spectra are elevated one order of magnitude above white noise, and KE approximately half an order of magnitude. Hence, for studying internal waves under various conditions, the w spectrum is more useful. The different effects of varying conditions on internal waves will become clear from a compilation of historic w spectra in the next section. Thereby, the flat white-noise spectrum Φ_e of the ADCP's "error" velocity is used for reference.

4. A compilation of previously observed vertical current spectra

The few reported open-ocean vertical current spectra show varying results. Pinkel's (1981) near-surface Φ_w inferred from isotherm displacements shows a nearly flat spectrum $\sim \sigma^0$ away from inertial and buoyancy frequencies, commensurate with equation (4). Near $\sigma = N$, however, the spectrum includes a small peak in variance $\Phi_{w,\mathrm{peak}}$, $\sigma_{\mathrm{peak}} \approx N$ (see also observations by Cairns and Williams [1976] and the theoretical description by Munk [1980] for an ocean with stratification only varying on the large scale, in which Airy functions are used to describe internal reflection at turning depths of a waveguide in an ocean with smoothly varying stratification). It can be inferred from Pinkel's Figure 2 that over half a frequency decade, the slope leading to this half a decade high near-N variance peak was $\sim\sigma^{+1}$ as in equation (6b). Stratification dependence was not verified by Pinkel.

Using temperature data from ∼1,400 m where $N >> f$ in the open Canary Basin (CB), northeast Atlantic, van Haren and Gostiaux (2009) found a σ^{+1} slope as in equation (6b) but also found that it extends throughout the entire internal wave continuum frequency

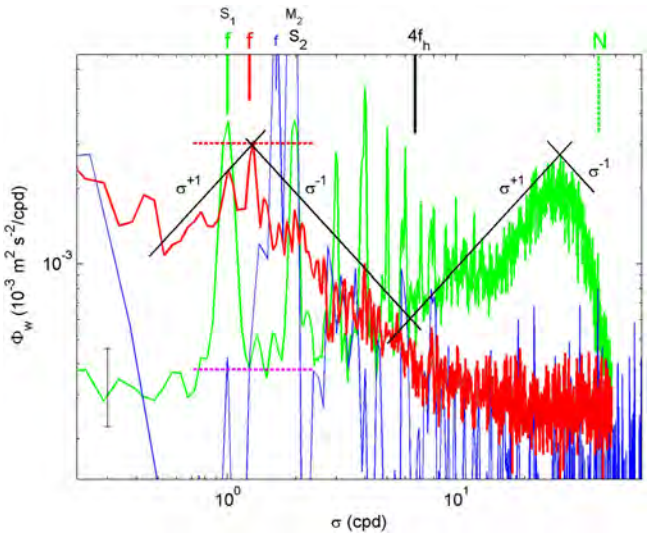

Figure 2. A composite vertical current spectrum (red/green) using 75 kHz acoustic Doppler current profiler (ADCP) data from two different deep-sea regions: green spectrum includes data from the Canary Basin, open northeast Atlantic Ocean (30° N, 27° W; 1,100 m in 4,500 m water depth, with associated value of N indicated by the vertical dashed line; the spectral spikes, already harmonically filtered, are at multiples of the diurnal frequency S_1, S_2, ... They are due to nonsinusoidal vertical plankton motions); red spectrum includes data from the Algerian Basin, open western Mediterranean Sea (38° N, 8° E; 2,400 m in 2,840 m water depth). The level of Φ_w at $\sigma = f$ is indicated by the red dashed horizontal line. For comparison, the blue spectrum in the background is for 600 kHz ADCP data from the shallow North Sea (54° N, 4° E; 25 m in 45 m water depth). The white-noise level for all spectra is indicated by the purple dashed line. The black vertical bar indicates the 95% confidence levels of random statistical significance. cpd, cycles per day.

range between f and N in contrast with equation (6b). The data from 2.5 m vertically separated sensors showed very few turbulent overturns, which may be expected considering the relatively strong stratification. Using the $O(100$ m) vertically averaged displacements of isopycnals, their "large-scale" Φ_w also showed a σ^{-1} slope as in equation (6a) for frequencies higher than those of the near-N peak, but over a frequency range of less than half a decade, before the slope became steeper, eventually becoming σ^{-3}. As the vertical range of observations was only 130 m, the range of stratification levels was insufficient to determine dependence on N.

These temperature-inferred w spectra were confirmed using direct vertical current observations from an upward-looking 75 kHz ADCP in the top of the same CB mooring (Fig. 2, green). The ADCP measures currents averaged over relatively small vertical scales of 10 m and relatively large horizontal scales of $O(100$ m). Compared with the temperature observations, the ADCP range was considerably larger in the vertical, $\sim$500 m over which N

varied by 30% to 40%. The spectra were observed to shift their $\Phi_{w,\mathrm{peak}}$ in frequency, in linear proportion with N changes (van Haren 2008c). The $\Phi_{w,\mathrm{peak}}$ was found at $\sigma_{\mathrm{peak}} = N$ minus one standard deviation of its variability around the large-scale mean. This frequency just below N is approximately one-half the buoyancy frequency measured with 10 m sensor spacing. The possibility that the variance of the $\Phi_{w,\mathrm{peak}}$ might vary with N was not investigated by van Haren (2008c).

In the green spectrum, representing CB's ADCP Φ_w (Fig. 2), the spikes at solar diurnal and its higher harmonic frequencies should be disregarded for the present analysis, as they are entirely attributable to vertical plankton motions. This is because (van Haren 2007) of the following: (1) no diurnal peak was visible in the horizontal current spectra, indicating that diurnal tides are not dominant; (2) similar peaks were visible in echo intensity that are dominated by reflections off zooplankton; and (3) the diurnal vertical migrations have the shape of a rectangular function that Fourier transforms to a series of higher harmonics (Fig. 1a). In contrast, the internal wave contribution to the spectrum is more broadband and is therefore easily distinguished.

The CB spectra are quite different from spectra inferred from observations in the deep western Mediterranean Sea (WM; red spectrum in Fig. 2; replicated from van Haren and Millot 2005) and the North Sea (NS; blue spectrum in Fig. 2; replicated from van Haren 2008b). The Φ_w from both latter areas is observed to exceed, at the 95% level of significance, the white-noise variance for $\sigma < 7$ cpd.

In the WM spectrum, the nearly constant slope of σ^{-1} for the frequency band $1.5 < \sigma < 7$ cpd seems interrupted by a statistically nonsignificant gap around $\sigma \approx 3$ cpd. The shipborne CTD-observed stratification amounted to $N = 0$ at the depth of the moored observations; however, 300 m higher up, $N \approx 3 \pm 1$ cpd, and in thin layers, $N \approx 6 \pm 2$ cpd $\approx N_m$ here (van Haren 2008a). At approximately N_m, the high- or low-frequency "peaks" drop off into noise: for vertical motions in weakly stratified waters, noise occurs for $\sigma > N_m$ (Fig. 2, red spectrum) and in strongly stratified waters for $\sigma < N_m$ (Fig. 2, green). This buoyancy frequency N_m equals $4 f_h = 6.5$ cpd to within one standard deviation.

WM's (red Φ_w) relatively broad near-inertial peak extends to subinertial frequencies in such a way that the slope is approximately σ^{+1} for $0.5 < \sigma < 1.3$ cpd. The lower bound of this frequency band is equivalent to the lower bound of the inertia-gravity wave band for very weak stratification with buoyancy frequency $O(f)$. This band thus includes freely propagating subinertial waves (e.g., LeBlond and Mysak 1978). The extent of the w spectrum into even lower frequencies $\sigma < 0.5$ cpd is not directly related to internal wave motions, but associated with mesoscale eddies and the corresponding horizontal density gradients in fronts.

Most importantly, the weakly stratified WM and NS Φ_w spectra not only have their peak frequency near f, instead of near N as observed in the stronger-stratified CB, but their peak variance also varies with N. Although the near-inertial peak in the WM data has the same variance as the near-N peak in the CB data, the near-inertial peak in the data from the slightly stronger-stratified NS near the bottom stands out above these two.

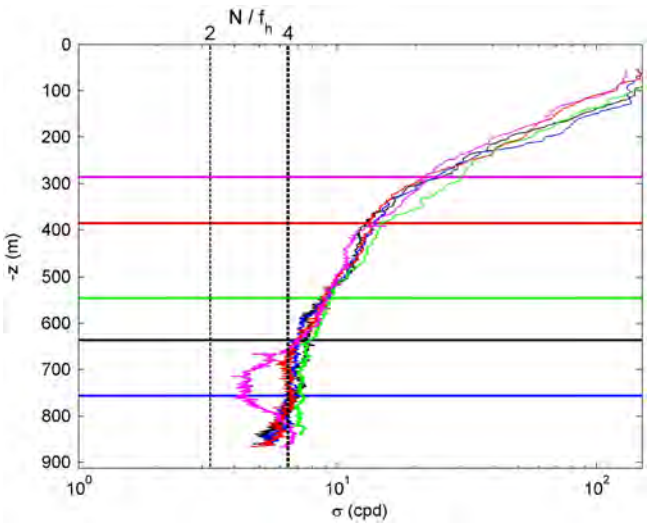

Figure 3. Large-scale buoyancy frequency ($\Delta z = 100$ m), also scaled with horizontal Coriolis parameter f_h (top axis), computed for five different conductivity-temperature-depth profiles near the acoustic Doppler current profiler (ADCP) mooring in the central-north Alboran Sea, western Mediterranean. The width and height of the total of different profiles indicate the approximate standard deviation in N computation. The five colored horizontal lines indicate depth levels of ADCP data (Fig. 4) for which spectra are computed in Figure 6. cpd, cycles per day.

At a first glance, this suggests for near-homogeneous waters a positive power law in N: $\Phi_w(\sigma, N) \propto N^p \sigma^{-1}$, $p > 0$, for the frequency range $f < \sigma < N$. This is best modeled using equation (8) for nonequilibrium internal wave fields (Phillips 1966), and quite different from the equilibrium and semiequilibrium CB spectra. The transition between the two different-equilibrium internal wave regimes is investigated in the next section using a recent data set from the central-north AS, where stratification varies from weak to strong across the depth range resolved by the ADCP.

5. Observing the transition from weakly to stronger-stratified waters

Over the 9 days of observations from the AS, the five CTD profiles show a gradual decrease in buoyancy frequency from ~23 cpd near the top of the ADCP range to a saturation level at ~6–7 cpd (Fig. 3). The latter is reached at ~630 m, well within the range of the ADCP. The nearly uniform stratification level found below 630 m has buoyancy frequency $N = 5.8 \pm 1$ cpd, or $N/f_h = 4 \pm 0.7$. Within the weakly stratified layer, a second saturation level is noticed at $N/f_h \approx 2.5$ in one profile of these large-scale Nvalues. The transition from weak to strong stratification seem smooth, although smaller-scale interfacial steps and

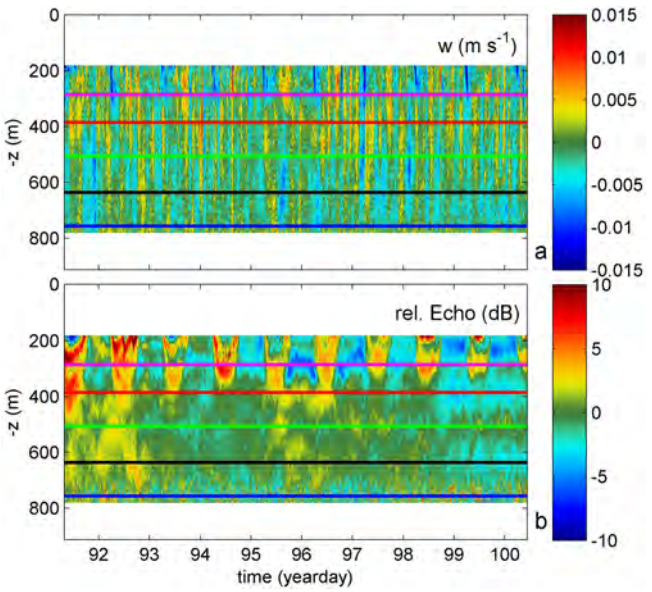

Figure 4. Depth-time images over the entire range of 75 kHz acoustic Doppler current profiler data from the central-north Alboran Sea. The five colored horizontal lines indicate depth levels for which Φ_w spectra are computed in Figure 6. (a) Vertical current, smoothed over 20 min intervals to reduce noise. (b) Raw relative echo amplitude.

homogeneous layers are obscured because of the coarse resolution ($\Delta z = 100$ m) used to compute N.

This transition appears different in time series of vertical motions (Fig. 4a). Although vertically coherent motions dominate, there are more intense layers (e.g., between the red and green horizontal lines) than elsewhere (e.g., between the black and blue lines), implying different vertical length scales for different vertical motions. This is more clearly visible in the 1-day zoom of Figure 5. It is noted that signals at the greatest observational depths, below the black line, are relatively noisy due to instrumental effects and fewer scatterers (see the noise in echo amplitude in Fig. 4b). Also note that the w signal appears to be dominated by lower frequencies above 350–400 m. This is because of diurnal vertical zooplankton motions, which are more visible in the echo amplitude (Fig. 4b). These plankton motions extend to ~400 m (the red line), although being somewhat variable and on days 92–93 perhaps extending down to 500 m (the green line). In the echo amplitude, we also note plankton attracted by interfacial layers that are moved by internal waves; see, for instance, the 100 m crest-trough variations around the green line at days 97–100.

At the colored line levels, we observe in CTD data (Fig. 3) a variation from $N = 6$ cpd so that $N/f_h = 4$ (blue, occasionally going down to $N = 3.5$ cpd, and black, the edge of

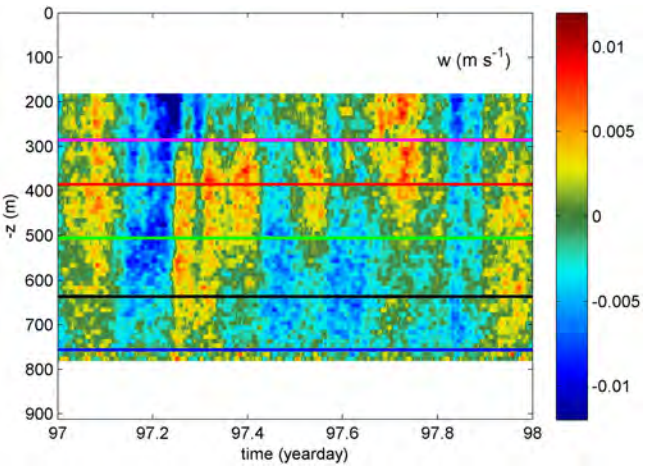

Figure 5. One-day zoom of Figure 4(a), with slightly different color scale.

the $N = 6$ cpd zone), via $N = 7$ cpd (green, to which the $N = 6$ cpd layer occasionally extends) to $N = 11$ cpd (red) and 32 cpd (purple). These variations in stratification are reflected in the vertical current time series of Figures 4(a) and 5 that show higher-frequency w motions with decreasing depth. Some properties will be revisited in the vertical current spectra.

The associated Φ_w spectra are presented in Figure 6. Because of the relative shortness of the record, the spectra are weakly smoothed to retain sufficient resolution. We observe the near-inertial peak variance to be a factor of 2 larger than that of the WM (the red dashed level is reproduced from Fig. 2). The value of Φ_w at $\sigma = f$ increases by a factor of 3 between the blue and black spectra. At other levels (other colors), the value at $\sigma = f$ slowly decreases in the direction of the surface.

At 750 m (blue spectrum), the peak is more or less flat. It extends to subinertial frequencies (not shown). In contrast, the spectrum at 630 m (black) has a slope close to σ^{+1} for $\sigma < 1.4$ cpd, its approximate peak frequency, and σ^{-1} for $1.4 < \sigma < 7$ cpd, where local $N = 7$ cpd. From 630 to 290 m (black to purple), this peak shifts to higher frequencies. (This is not clearly visible for the purple spectrum, which is dominated by the diurnal and higher harmonic plankton motions; Fig. 4.) With this shift to higher frequencies, the level at f decreases for increasing N (except for the purple spectrum). More clearly, a σ^{+1} slope appears for $\sigma < 0.5N$ (the approximate peak frequency) and a σ^{-1} slope for $\sigma > 0.5N$. With the variance values at $\sigma = f$, the values at σ_{peak} also decrease for increasing N, with the exception of the red spectrum at 390 m (red). Thus, a smooth spectral transition is observed between the weakly and strongly stratified regimes with the largest variance at the depth where $N/f_h = 4$ (i.e., ~630 m; black spectrum). These unique w-spectral

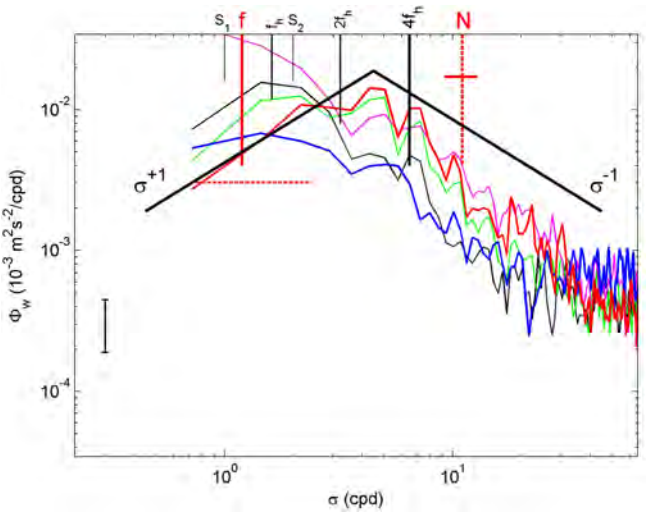

Figure 6. As Figure 2, but for spectra from different depths of Alboran Sea acoustic Doppler current profiler (ADCP) data of Figure 4(a). The indicated buoyancy frequency is computed from conductivity-temperature-depth data (Fig. 3) for the red depth level. Its ADCP spectral peak lies near $0.5N$. The horizontal red dashed line is the peak level of the red spectrum in Figure 2, used for reference here. The black vertical bar indicates the 95% confidence levels of random statistical significance. cpd, cycles per day.

observations under background conditions varying from weak to strong stratification are used in the next section to construct a composite spectrum for all conditions. This composite spectrum is further extended with observations from Section 4.

6. Construction of a composite vertical current peak spectrum

With reference to the value of the WM peak variance (the red dashed line in Figs. 2 and 6), the internal waves' vertical current peak variance is found to form a triangle in log-log space as a function of local conditions N scaled by f_h (Fig. 7). This scaling is employed here to generalize for different (mid-)latitudes. We use $N = (2-0.7)\,f_h = 1.3\,f_h$ to replace the local $N = 0$ for the stratification in the WM data. In the NS, the weakest stratification in the bottom boundary layer determines the internal waves in the pycnocline above it (van Haren 2008b), and the minimum N value in a 100 m range also fits the present observations best here. This replacement-stratification value is justified by the spectral information, considering the peak frequency $\sigma_{\text{peak}} \approx 0.5N$. The spectral values of Figure 2 are given by their colors (red, blue, and green) and with empty circles for weak stratification ($N/f_h < 4$) and plus signs for strong stratification ($N/f_h > 4$). The observational AS data from Figure 6 are added after visually determining the peak frequency and by using $N - 0.7\,f_h$, which

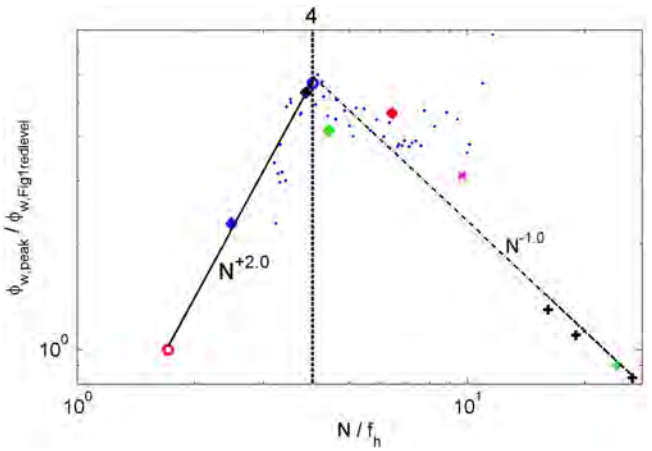

Figure 7. Relationships between large-scale N stratification, scaled with the horizontal Coriolis parameter, and the ratio variance of peak vertical current spectra with reference to that of the deep Mediterranean (dashed red level in Figs. 2 and 6). Data from Figure 2 are indicated by their colors (red and blue empty circles and green plus sign). Data from Figure 6 are also indicated by their colors (blue, black, green, and red diamonds and purple cross). Black plus signs are inferred from additional strongly stratified open-ocean data. Blue dots are from 56 depth levels of Alboran Sea acoustic Doppler current profiler data by automatically selecting the absolute peak variance (frequency).

is approximately equivalent to using the N from 50 m below the observational depth, or the minimum in the variations across the range of 100 m for computing N. The colors are identical to those of the five lines in Figures 3–6, using large diamonds as symbols here, except for the purple cross indicating inaccurate data due to diurnal plankton motions. With the exception of the purple cross, all data are then used to linearly fit two different lines, as indicated,

$$\Phi_{w,\mathrm{peak}}(N/f_h) \propto N^2, \qquad N/f_h < 4, \sigma_{\mathrm{peak}} = f - f_h \tag{9a}$$

$$\Phi_{w,\mathrm{peak}}(N/f_h) \propto N^{-1}. \qquad N/f_h > 4, \sigma_{\mathrm{peak}} = 0.5 - 0.7N \tag{9b}$$

These fits to the observations are confirmed with additional data from three other depths in the CB (black plus signs) and with data from all other depths in the AS (blue dots), outside the noisy-data range. These AS data are automatically selected as the frequency of the absolute peak in a spectrum. For finding the corresponding local N, all five CTD profiles were averaged. The resulting blue dots clearly deviate from the dashed straight-line fit for $N/f_h > 4$ halfway between the red diamond and purple cross. This is attributable to the effects of zooplankton motions contaminating the automated search for spectral peaks. For

$N/f_h < 4$, the deviation from the straight solid line halfway between the blue and black diamonds is related with the limited observation of very weak stratification.

However, these data do show that the largest $\Phi_{w,\text{peak}}$ is found at $N/f_h = 4$. These observations add to the observations of the shape of the spectral peaks and their σ dependence (Figs. 2 and 6),

$$\Phi_w(\sigma) \propto \sigma^{+1}, \qquad [0.5f - f <]\sigma < \sigma_{\text{peak}} \tag{9c}$$

$$\Phi_w(\sigma) \propto \sigma^{-1}. \qquad \sigma_{\text{peak}} < \sigma[< N] \tag{9d}$$

7. Discussion

The present overview of observations demonstrates internal wave fields that are not dominantly found in equilibrium. The well-stratified open-ocean (and open-sea) internal wave fields are found in (semi-)equilibrium, with $\Phi_{w,\text{peak}} \sim N^{-1}$ as in equation (4), but $\Phi_w(\sigma) \sim \sigma^{+1}$ for $\sigma < N$ and $\Phi_w(\sigma) \sim \sigma^{-1}$ for $\sigma > N$, as in equations (6a) and (6b). In actively varying internal wave fields in near-homogenous waters of the Mediterranean Sea and NS, Φ_w spectra are found to represent a nonequilibrium internal wave field as in equation (8). Previously, the latter were attributed to nonlinear motions (van Haren 2008b). Internal waves smoothly couple between the regimes as is observed near the top of Figure 7.

In the NS, the strong tidal friction creates sufficient turbulence to homogenize the bottom boundary layer up to half the water column, twice a tidal period. This causes similar water mass characteristics as in the deep Mediterranean, with low stratification of the same order of magnitude. It is thus not surprising that these waters, upon relaxation of horizontal density gradients, carry internal waves, occasionally. From the spectra, it is inferred that these internal waves transfer part of their variance to lower-frequency near-inertial waves, at which Φ_w peaks.

Near-inertial waves are considered to be generated via geostrophic adjustment, basically creating horizontal circular motions in strongly stratified waters (e.g., Gill 1982). In very weak stratification, these motions can obtain a vertical component with an aspect ratio of $O(1)$ (LeBlond and Mysak 1978; van Haren and Millot 2005). This variation in near-inertial motions orientation could be simply interpreted as $\Phi_w \sim N^p$, $p < 0$ at $\sigma = f$, which expresses the weaker stratification to allow a relatively larger vertical component. Such a relationship is indeed as observed here, but for $N/f_h > 4$ only. However, the inverse relationship $p > 0$ is observed for $N/f_h < 4$. This may be interpreted as an increase in adjustment activity instead of a settling into a quiescent horizontal layering of density. The energy transfer to $\sigma = f$ is necessary in a generally near-homogeneous background because only inertial waves can propagate freely from stratified to homogeneous layers. This has consequences for vigorous vertical convective overturning generation via inertial motions, as observed in the deep Mediterranean using high-resolution temperature sensors (van Haren and Gostiaux 2011).

Compared with the near-homogeneous Mediterranean and NS areas, the strongly stratified open ocean is characterized by relatively weak diapycnal turbulent mixing. This weak mixing occurs intermittently in sparse patches with mostly laminar motions in between, as suggested by Turner (1979). The observed difference in spectra is hypothesized to be associated with these variations in diapycnal turbulent mixing. In that case, the balance between shear and stratification, governing the turbulence dissipation rate, would also reflect the large-scale forcing when it balances the dissipation.

The combined, different and complimentary, spectra under strong- and weak-stratified conditions are examples for a probably wide range of seas and oceans. By their deviation from an equilibrium internal wave spectrum, they may be useful as a reference for the dynamic process of internal wave–induced turbulent mixing in the ocean. The AS data demonstrate that the combined spectra can be found in one and the same area, although not at the same depths, suggesting a smooth spectral but abrupt depth transition. The transition frequency of $4\,f_h$ has previously been observed to naturally limit small-scale minimum stratification and maximum shear, with respect to convective "homogeneous" layers (van Haren 2008a). (Under linear stability conditions, $N/f_h = 2$ would be a limit.) The $N/f_h = 4$ thus implies a transition from large-scale (sub-)inertial convective overturning in gyroscopic wave–dominated dynamics (for $N/f_h < 4$) to (interfacial) gravity wave–dominated dynamics (for $N/f_h > 4$). In other words, it indicates a transition from a vertical- to a horizontal-layered ocean.

Acknowledgments. I acknowledge the Netherlands Organisation for the Advancement of Scientific Research (NWO) for support. I thank two anonymous reviewers for their constructive comments on an earlier draft.

REFERENCES

Cairns, J. L., and G. O. Williams. 1976. Internal wave observations from a midwater float, 2. J. Geophys. Res., *81*, 1943–1950.

Fofonoff, N. P. 1969. Spectral characteristics of internal waves in the ocean. Deep-Sea Res., *16*(Suppl.), 58–71.

Garrett, C., and W. Munk. 1972. Space-time scales of internal waves. Geophys. Fluid Dyn., *3*, 225–264.

Garrett, C., and W. Munk. 1979. Internal waves in the ocean. Annu. Rev. Fluid Mech., *11*, 339–369.

Gill, A. E. 1982. Atmosphere–Ocean Dynamics. Orlando, FL: Academic Press, 662 pp.

Howard, L. N. 1961. Note on a paper of John W. Miles. J. Fluid Mech., *10*, 509–512.

LeBlond, P. H., and L. A. Mysak. 1978. Waves in the Ocean. Amsterdam: Elsevier, 602 pp.

Linden, P. F. 1979. Mixing in stratified fluids. Geophys. Astrophys. Fluid Dyn., *13*, 3–23.

Miles, J. W. 1961. On the stability of heterogeneous shear flows. J. Fluid Mech., *10*, 496–508.

Miropol'sky, Y. Z. 2001. Dynamics of Internal Gravity Waves in the Ocean. Dordrecht, The Netherlands: Kluwer, 406 pp.

Munk, W. 1981. Internal waves and small-scale processes, *in* Evolution of Physical Oceanography, B. A. Warren and C. Wunsch, eds. Cambridge, MA: MIT Press, 264–291.

Munk, W. H. 1980. Internal wave spectra at the buoyant and inertial frequencies. J. Phys. Oceanogr., *10*, 1718–1728.

Parks, T. W., and C. S. Burrus. 1987. Digital Filter Design. New York: Wiley, 342 pp.

Phillips, O. M. 1966. The Dynamics of the Upper Ocean. Cambridge: Cambridge University Press, 261 pp.

Pinkel, R. 1981. Observations of the near-surface internal wavefield. J. Phys. Oceanogr., *11*, 1248–1257.

Turner, J. S. 1979. Buoyancy Effects in Fluids. Cambridge: Cambridge University Press, 368 pp.

van Haren, H. 2007. Monthly periodicity in acoustic reflections and vertical motions in the deep ocean. Geophys. Res Lett., *34*, L12603. doi: 10.1029/2007GL029947

van Haren, H. 2008a. Abrupt transitions between gyroscopic and internal gravity waves: The mid-latitude case. J. Fluid Mech., *598*, 67–80.

van Haren, H. 2008b. A comparison between vertical motions measured by ADCP and inferred from temperature data. Ocean Sci., *4*, 215–222.

van Haren, H. 2008c. Self-regulation of deep-ocean internal wave continuum: Observations on related near-inertial shear and high-frequency vertical motions. Geophys. Res. Lett., *35*, L04606. doi: 10.1029/2007GL032697

van Haren, H., and L. Gostiaux. 2009. High-resolution open-ocean temperature spectra. J. Geophys. Res.: Oceans, *114*, C05005. doi: 10.1029/2008JC004967

van Haren, H., and L. Gostiaux. 2011. Large internal waves advection in very weakly stratified deep Mediterranean waters. Geophys. Res. Lett., *38*, L22603. doi: 10.1029/ 2011GL049707

van Haren, H., and C. Millot. 2005. Gyroscopic waves in the Mediterranean Sea. Geophys. Res. Lett., 32, L24614. doi: 10.1029/2005GL023915

Wunsch, C. 1975. Deep ocean internal waves: What do we really know? J. Geophys. Res., *80*, 339–343.

Received: *21 January 2014*; revised: *20 January 2015*.